https://doi.org/10.2352/ISSN.2470-1173.2018.15.COIMG-103

Ultrasonic Model-Based Iterative Reconstruction with Spatially Variant Regularization for One-Sided Non-Destructive Evaluation

Hani Almansouri[1], Singanallur Venkatakrishnan[2], Dwight Clayton[2], Yarom Polsky[2], Charles Bouman[1], and Hector Santos-Villalobos[2]

[1]Purdue University, 610 Purdue Mall, West Lafayette, IN 47907
[2]Oak Ridge National Laboratory, One Bethel Valley Road, Oak Ridge, TN 37831

Abstract

One-sided ultrasonic non-destructive evaluation (UNDE) uses ultrasound signals to investigate and inspect structures that are only accessible from one side. A widely used reconstruction technique in UNDE is the synthetic aperture focusing technique (SAFT). SAFT produces fast reconstruction and reasonable images for simple structures. However, for large complex structures, SAFT reconstructions suffer from noise and artifacts. To resolve some of the drawbacks of SAFT, an ultrasonic model-based iterative reconstruction (MBIR) algorithm, a method based on Bayesian estimation, was proposed that showed significant enhancement over SAFT in reducing noise and artifacts. In this paper, we build on previous investigations of the use of MBIR reconstruction on ultrasound data by proposing a spatially varying prior-model to account for artifacts from deeper regions and a 3D regularizer to account for correlations between scans from adjacent regions. We demonstrate that the use of the new prior model in MBIR can significantly improve reconstructions compared to SAFT and the previously proposed MBIR technique. [1]

Introduction

One-sided Non-destructive evaluation (NDE) is used to characterize structures that are only accessible from one side without destroying or physically modifying the structures. Ultrasound is one of the NDE methods which is used when portability, cost, and radiation dose matter. One of the applications of one-sided ultrasonic NDE (UNDE) is in inspecting large concrete structures in power plants to detect the early stages of degradation. For example, nuclear power plants (NPP) contain heavily reinforce concrete structures that act as a shield against radiation [1]. These structures degrade with time due to many reasons, such as radiation, temperature, or contact with water, salt, or chemicals. Early detection of degradation is very important because it allows the damage to be repaired resulting in an extended operation life. Otherwise, flaws in the concrete and steel structures might jeopardize the safe operation of the NPP. Similarly, geothermal and oil and gas production wells contain concrete structures that must be maintained and managed to prevent unwanted leakage and maintain well performance [2, 3]. The current techniques used for one-sided UNDE are either fast with low resolution images or computationally expensive and consequently not practical for in-the-field or real-time assessment. Therefore, locating defects through one-sided UNDE is still a challenging problem.

A widely used technique for one-sided UNDE is the synthetic aperture focusing technique (SAFT) [4, 5, 6, 7, 8]. SAFT is more practical than other techniques because it is fast and produces acceptable images. However, for complex structures, SAFT images suffer from noise, low resolution, and artifacts due to surface waves, reverberation, diffraction, and other non-linear effects which make it hard to interpret the image. An example of SAFT reconstruction is shown in Fig. 1.

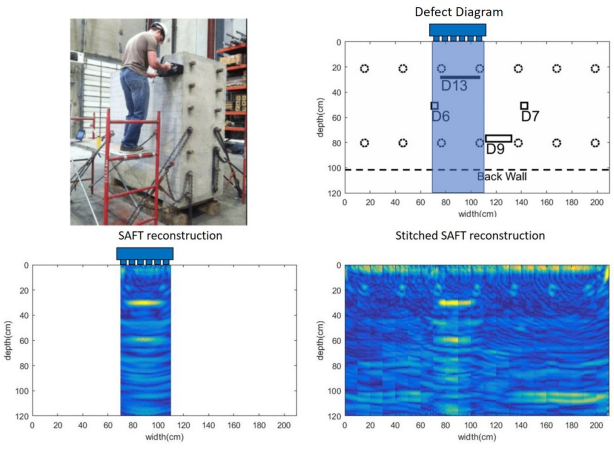

Figure 1. *An example of SAFT reconstruction. The top left image shows experimental data extracted from a large concrete structure [9].The top right image shows the defect diagram of a cross section of the concrete structure that contain some defects (rectangular shape) and some steel rebars (circular shape). The bottom left image shows SAFT reconstruction of a small region in the cross section. The bottom right image shows SAFT reconstruction of multiple images stitched together to show the full region.*

The reconstruction quality can be significantly improved compared to SAFT by using model-based/regularized iterative

[1]This manuscript has been authored by UT-Battelle, LLC under Contract No. DE-AC05-00OR22725 with the U.S. Department of Energy. The United States Government retains and the publisher, by accepting the article for publication, acknowledges that the United States Government retains a non-exclusive, paid-up, irrevocable, world-wide license to publish or reproduce the published form of this manuscript, or allow others to do so, for United States Government purposes. The Department of Energy will provide public access to these results of federally sponsored research in accordance with the DOE Public Access Plan (http://energy.gov/downloads/doe-public-access-plan).

methods that obtain the reconstruction by minimizing a cost function that balances a data-fidelity term and a regularization term that enforces certain constraints on the image to be reconstructed. An ultrasonic model-based iterative reconstruction (MBIR) technique was proposed to overcome some of the issues in SAFT and showed significant improvements in reducing noise and artifacts compared with SAFT [10, 11]. However, the model did not account for attenuation of deeper reflections due to dramatic reduction in signal strength and a loss of resolution due to the geometry of the set-up. It also did not exploit correlations from adjacent 2D cross sections when inspecting large structures that require raster scanning the device and making measurements over the entire structure.

In this paper, we present an algorithm for UNDE reconstruction that enhances the well known prior model/regularizer in the MBIR framework. We modify the model to account for artifacts in deeper regions by applying a spatially variant regularization (SVR). The spatially variant regularization is used to reduce the regularization for voxels which are at a greater depth from the transducer than the ones closer to the transducer. We also modify the prior-model to account for correlations between adjacent cross-sections in a raster scan by coupling the voxels by using a 26-point "3D" neighborhood system. This second feature further reduces noise and artifacts in the reconstruction. We demonstrate that the proposed MBIR algorithm can produce higher quality reconstructions than SAFT and the conventional MBIR method by suppressing noise and artifacts.

Ultrasonic MBIR

In this section, we summarize the previously proposed MBIR method in [11]. The MAP estimate used in MBIR is given by

$$x_{\text{MAP}} = \arg\min_x \{f(x)\} \quad (1)$$

$$= \arg\min_x \{-\log p(y|x) - \log p(x)\}, \quad (2)$$

where $f(x)$ is the MAP cost function, y is the measurements or data, and x is the image to be reconstructed, $p(y|x)$ is the probability density function of the measurements given the unknown image (forward model) and $p(x)$ is the pdf of the image (prior model).

First, in order to design the forward model, we assumed that the medium is linear. With this assumption y can be related to x by the following equation,

$$y = Ax + Dg + w,$$

where A is the system matrix, D is the surface wave model [11], g is a scaling coefficient vector for D, and w is an i.i.d Gaussian vector with distribution $w \sim \mathcal{N}(0, \sigma^2 I)$. Hence,

$$-\log p(y|x) = \frac{1}{2\sigma^2} \|y - Ax - Dg\|^2 + \text{constant}.$$

As shown in Fig. 2, A is computed by considering a signal transmitted from transducer i at location $r_i \in \mathbb{R}^3$, reflected by point $v \in \mathbb{R}^3$, and received from transducer j located at $r_j \in \mathbb{R}^3$.

Next, we adopted the q-generalized Gaussian Markov random field (QGGMRF) for the prior model [12]. With this design,

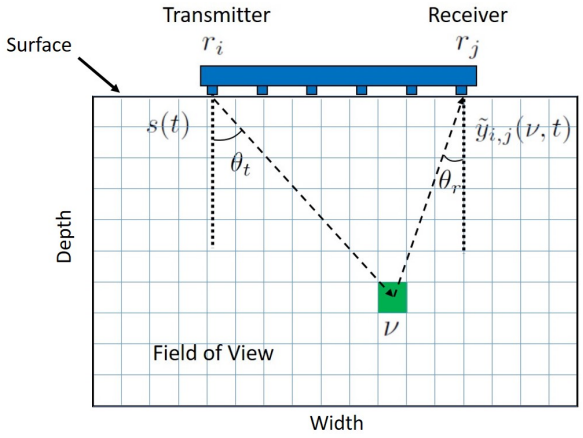

Figure 2. *An illustration of a typical ultrasonic one-sided NDE problem where $s(t)$ is the transmitted signal, v is a point in the field of view, $y_{i,j}(v,t)$ is the received signal reflected from v, θ_t is the angle between r_i and v, and θ_r is the angle between r_j and v.*

the prior model is

$$p(x) = \frac{1}{z} \exp\left(- \sum_{\{s,r\} \in C} b_{s,r}\, \rho(x_s - x_r) \right), \quad (3)$$

where z is a normalizing constant, C is the set of pair-wise cliques, and

$$\rho(\Delta) = \frac{|\Delta|^p}{p\sigma_x^p} \left(\frac{|\frac{\Delta}{T\sigma_x}|^{q-p}}{1 + |\frac{\Delta}{T\sigma_x}|^{q-p}} \right). \quad (4)$$

Hence,

$$-\log p(x) = \sum_{\{s,r\} \in C} b_{s,r}\, \rho(x_s - x_r) + \text{constant}. \quad (5)$$

Substituting the forward and prior models into Eq. 2,

$$(x,g)_{MAP} = \arg\min_{x,g} \left\{ \frac{1}{2\sigma^2} \|y - Ax - Dg\|^2 + \sum_{\{s,r\} \in C} b_{s,r}\, \rho(x_s - x_r) \right\}. \quad (6)$$

Eq. 6 is optimized using the iterative coordinate descent algorithm (ICD) and the majorization technique [11].

Spatially Variant Regularization

The MBIR model shown above applies a spatially constant regularization (SCR) over the whole field of view i.e. the values of $b_{s,r}$ only depend on the relative position of the voxel at r to the voxel at s. However, the use of such a model results in artifacts in the MBIR framework because of the higher attenuation of the signal and a broader system point spread function at greater depths, which are not fully accounted for by the forward model. An example of such artifacts in MBIR is shown in Fig. 3. To address such artifacts, we modify the prior model to be a function of depth where the regularization decreases as the depth increases. We apply an this spatially variant regularization (SVR) by replacing σ_x in Eq. 4 with $\sigma_{x_{s,r}}$ which is defined as

$$\sigma_{x_{s,r}} = \sigma_0 \sqrt{m_s m_r},$$

and

$$m_s = 1 + (m-1) * \left(\frac{\text{depth of pixel s}}{\text{maximum depth}} \right)^a, \tag{7}$$

where m_s is monotone increasing with respect to depth, σ_0 is equal to the old value of σ_x, $m \geq 1$, and $a \geq 0$. Fig. 4 shows a plot of Eq. 7 with respect to a where a controls how fast m is approached. We note that one drawback of this method is that it will amplify both the reflections and the noise in the deeper regions.

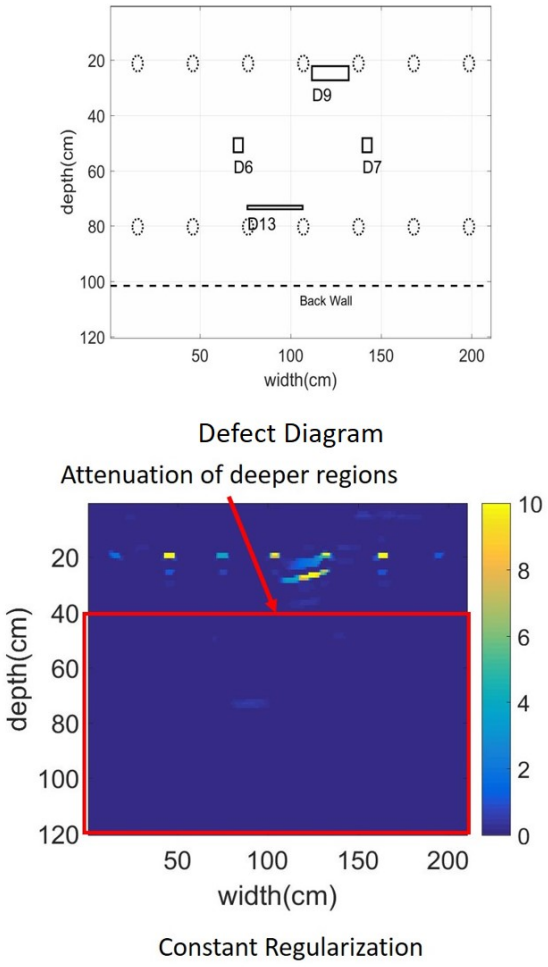

Figure 3. *An example of SCR-MBIR reconstruction where deeper regions suffer from significant attenuation.*

2.5D Ultrasonic MBIR

When inspecting a large field of view that requires raster scanning of multiple layers or cross sections, we can make use of the extra information from adjacent layers. This can help in further reduction of noise and artifacts in the reconstruction. In contrast to the work in [13], in this section, we modify $\beta_{s,r}$ for the neighbors around the pixel s in Eq. 6 to be

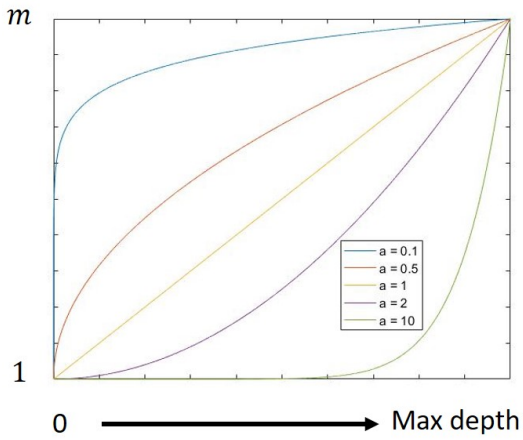

Figure 4. *Plots of m_s in Eq. 7 with different values of a.*

$$\begin{bmatrix} b_{s,r_1} & b_{s,r_2} & b_{s,r_3} \\ b_{s,r_4} & b_{s,r_5} & b_{s,r_6} \\ b_{s,r_7} & b_{s,r_8} & b_{s,r_9} \end{bmatrix} = \begin{bmatrix} 0 & 0 & 0 \\ 0 & 2 & 0 \\ 0 & 0 & 0 \end{bmatrix} \cdot \frac{\gamma}{4\gamma+12},$$

$$\begin{bmatrix} b_{s,r_{10}} & b_{s,r_{11}} & b_{s,r_{12}} \\ b_{s,r_{13}} & 0 & b_{s,r_{14}} \\ b_{s,r_{15}} & b_{s,r_{16}} & b_{s,r_{17}} \end{bmatrix} = \begin{bmatrix} 1 & 2 & 1 \\ 2 & 0 & 2 \\ 1 & 2 & 1 \end{bmatrix} \cdot \frac{1}{4\gamma+12},$$

$$\begin{bmatrix} b_{s,r_{18}} & b_{s,r_{19}} & b_{s,r_{20}} \\ b_{s,r_{21}} & b_{s,r_{22}} & b_{s,r_{23}} \\ b_{s,r_{24}} & b_{s,r_{25}} & b_{s,r_{26}} \end{bmatrix} = \begin{bmatrix} 0 & 0 & 0 \\ 0 & 2 & 0 \\ 0 & 0 & 0 \end{bmatrix} \cdot \frac{\gamma}{4\gamma+12},$$

where the middle equation shows the coefficient of the neighbors from the same layer, and the top and bottom equations shows the coefficient of the neighbors for the adjacent layers. The value $\gamma \geq 0$ controls the contribution from neighbors of adjacent layers.

Experimental Results

For the experimental results, a heavily reinforced large concrete structure was built with dimensions 84 x 84 x 40 inches [9]. Some defects were embedded in the structure at different positions to simulate real defects. An ultrasonic system, MIRA [14], was used to transmit and receive a signal with carrier frequency of 52 kHz and a sampling rate of 1 MHz using an array of 10 transducers. Fig. 5 shows some images of the structure, the type and position of the defects, and the MIRA device used. The whole block was divided into horizontal and vertical cross sections. Each cross section requires 18 scans from the MIRA device where each individual scan is shifted by 4 inches from its adjacent scans. Each scan data is reconstructed to produce an image with 40 cm width and 120 cm depth with pixels of of 1 cm (for both SAFT and MBIR). The acoustic speed and attenuation coefficient were set to 2,620 m/s and 30×10^{-6} $\frac{1}{m \cdot Hz}$, respectively.

Fig. 6 shows the enhancement of MBIR when spatially variant regularization and 2.5D MBIR is added to the model. The top left image shows the defect diagram. The top right image shows 2D spatially constant regularization MBIR (SCR-MBIR). The bottom left image shows 2D spatially variant regularization

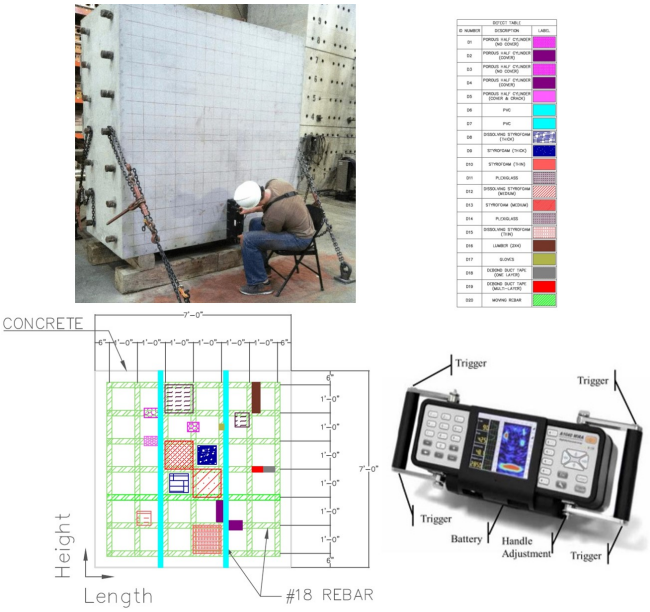

Figure 5. *The concrete block and ultrasound device used for the experimental data. The top left image shows a picture of the block while conducting the experiment using the MIRA device. The top right and bottom left images shows the type and position of the defects, respectively. The bottom right image shows the MIRA device used in the experiment [9].*

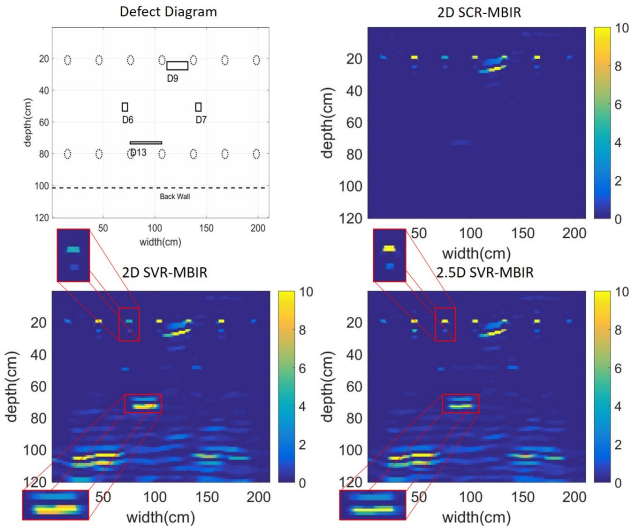

Figure 6. *A comparison between MBIR before and after applying SVR and 2.5D MBIR. The top left image shows the defect diagram. The top right image shows 2D SCR-MBIR. The bottom left image shows 2D SVR-MBIR. The bottom right image shows 2.5D SVR-MBIR.*

MBIR (SVR-MBIR). The bottom right image shows 2.5D SVR-MBIR. The 2D SVR-MBIR was able to amplify the deeper regions that were attenuated in the 2D SCR-MBIR. The 2.5D SVR-MBIR shows slightly better noise reduction and resolution enhancement than in 2D SVR-MBIR. As shown in Fig. 6, the regions at depth 80 cm or greater showed less noise. Also, visually the resolution appears to be improved for some targets, such as D13.

A comparison between SAFT and MBIR is shown in Fig. 7. The left column is the defect diagram. The middle column is the instantaneous envelope of SAFT reconstruction. The right column is 2.5D SVR-MBIR reconstruction. Each defect diagram is a cross section of the concrete block at a different region. The circle on the defect diagram are steel rebars perpendicular to the cross section. The squares are the embedded defects in the structure. The horizontal line at the bottom is the back wall of the structure. The results show improvement with MBIR over SAFT in reducing noise and artifacts in all results. MBIR , in general, shows improvements in identifying targets than SAFT. For example, the top steel rebars appear more clearly in MBIR. It is important to note that the position of the defects might have changed while pouring the cements. Therefore, the position shown in the defect diagram is our best guess of the true location. Also, some defects have very weak reflections that may not appear in either technique, such as D6 and D7 (PVC). Since SAFT and MBIR have different units, they don't show the same scaling.

Conclusion

In this paper, we demonstrated additional enhancements to the previously proposed MBIR [11]. We applied an SVR to the prior model to account for the artifacts at deeper regions of the region being inspected. We also applied a 3D regularizer in the MBIR framework to further reduce noise and artifacts and enhance resolution. We showed experimental results comparing SAFT, conventional MBIR, and proposed MBIR and showed further enhancement in the reconstruction, especially in reducing noise and artifacts, using the proposed technique. However, this enhancement comes at the cost of adding more parameters to the prior model, e.g. m, a, and γ.

References

[1] P. Ramuhalli, J. W. Griffin, R. M. Meyer, S. G. Pitman, J. M. Fricke, M. E. Dahl, M. S. Prowant, T. A. Kafentzis, J. B. Coble, and T. J. Roosendaal, *Nondestructive Examination (NDE) Detection and Characterization of Degradation Precursors, Technical Progress Report for FY 2012*. Washington, D.C. : United States. Office of the Assistant Secretary for Nuclear Energy ; Oak Ridge, Tenn. : distributed by the Office of Scientific and Technical Information, U.S. Dept. of Energy, 2012.

[2] M. Berndt, "Non-destructive testing methods for geothermal piping.," tech. rep., Brookhaven National Lab., Upton, NY (US), 2001.

[3] J. Zemanek, E. E. Glenn, L. J. Norton, and R. L. Caldwell, "Formation evaluation by inspection with the borehole televiewer," *Geophysics*, vol. 35, no. 2, pp. 254–269, 1970.

[4] Z. Shao, L. Shi, Z. Shao, and J. Cai, "Design and application of a small size saft imaging system for concrete structure," *Review of Scientific Instruments*, vol. 82, no. 7, p. 073708, 2011.

[5] B. J. Engle, J. L. W. Schmerr, and A. Sedov, "Quantitative ultrasonic phased array imaging," *AIP Conf. Proc.*, vol. 1581, no. 7, p. 49, 2014.

[6] G. Dobie, S. G. Pierce, and G. Hayward, "The feasibility of synthetic aperture guided wave imaging to a mobile sensor platform," *NDT and E International*, vol. 58, no. 7, pp. 10–17, 2013.

[7] S. Beniwal and A. Ganguli, "Defect detection around rebars in concrete using focused ultrasound and reverse time migration," *Ultrasonics*, vol. 62, pp. 112–125, 2015.

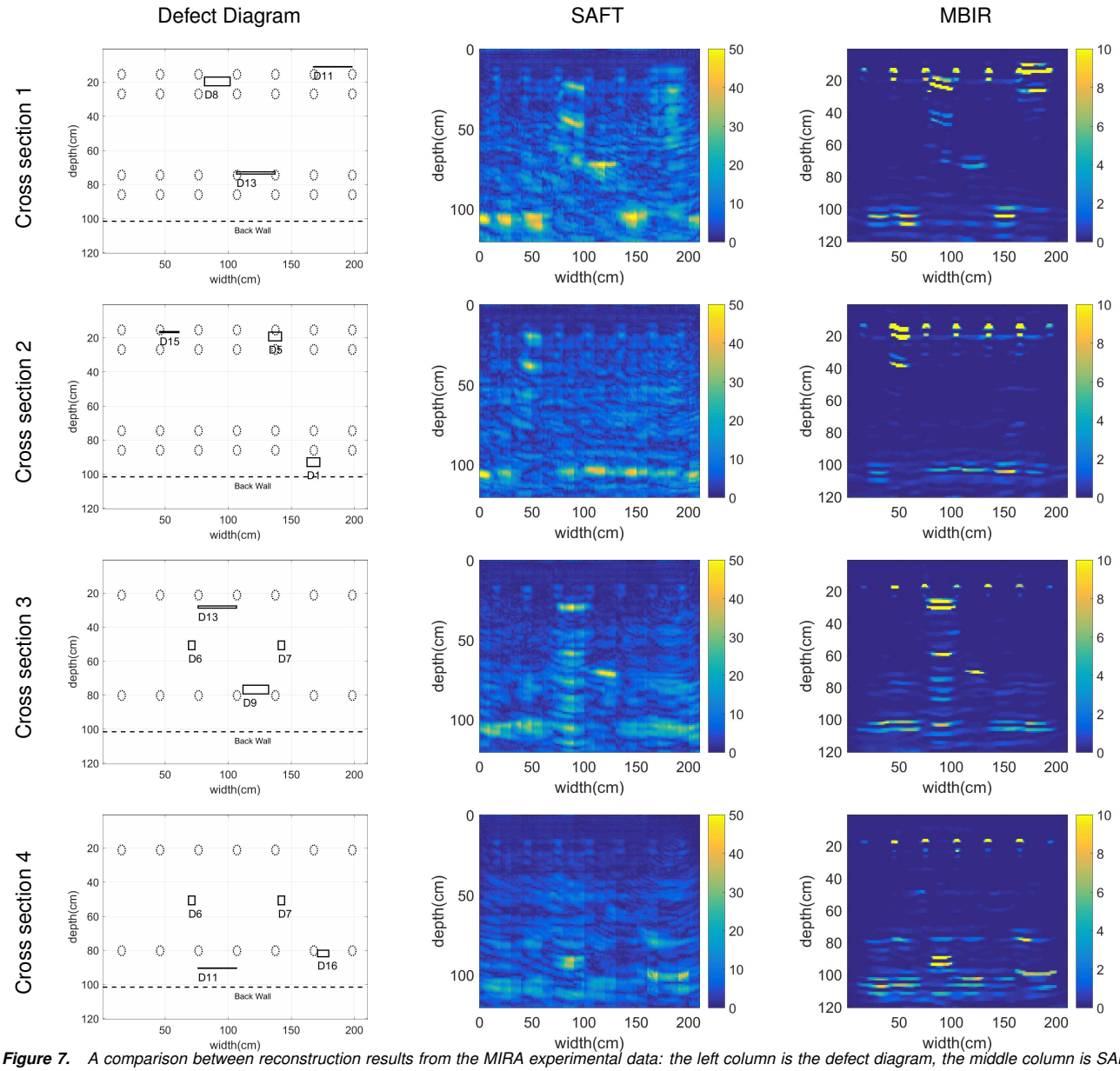

Figure 7. *A comparison between reconstruction results from the MIRA experimental data: the left column is the defect diagram, the middle column is SAFT reconstruction, the right column is 2.5D SVR-MBIR reconstruction. MBIR tends to produce results with less noise and artifacts compared to SAFT.*

[8] K. Hoegh and L. Khazanovich, "Extended synthetic aperture focusing technique for ultrasonic imaging of concrete," *NDT & E International*, vol. 74, pp. 33–42, 2015.

[9] D. A. Clayton, A. M. Barker, H. J. Santos-Villalobos, A. P. Albright, K. Hoegh, and L. Khazanovich, "Nondestructive evaluation of thick concrete using advanced signal processing techniques," tech. rep., Oak Ridge National Lab.(ORNL), Oak Ridge, TN (United States), 2015.

[10] H. Almansouri, D. Clayton, R. Kisner, Y. Polsky, C. Bouman, and H. Santos-Villalobos, "Development of acoustic model-based iterative reconstruction technique for thick-concrete imaging," in *AIP Conference Proceedings*, vol. 1706, p. 020013, AIP Publishing, 2016.

[11] H. Almansouri, C. Johnson, D. Clayton, Y. Polsky, C. Bouman, and H. Santos-Villalobos, "Progress implementing a model-based iterative reconstruction algorithm for ultrasound imaging of thick concrete," in *AIP Conference Proceedings*, vol. 1806, p. 020016, AIP Publishing, 2017.

[12] J.-B. Thibault, K. D. Sauer, C. A. Bouman, and J. Hsieh, "A three-dimensional statistical approach to improved image quality for multislice helical ct," *Medical physics*, vol. 34, no. 11, pp. 4526–4544, 2007.

[13] H. Almansouri, C. Johnson, D. Clayton, Y. Polsky, C. Bouman, and H. Santos-Villalobos, "Anisotropic modeling and joint-map stitching for improved ultrasound model-based iterative reconstruction of large and thick specimens," *to appear* in AIP Conference Proceedings, 2018.

[14] *ULTRASONIC LOW-FREQUENCY TOMOGRAPH 1040 MIRA OPERATION MANUAL*. Acoustic Control Systems, Ltd, 2015.

Author Biography

Hani Almansouri is currently a PhD student at Purdue University. He received his Bachelors and Masters degrees in Electrical and Computer Engineering from Purdue University, West Lafayette, IN in 2010 and 2013, respectively. His research interests are ultrasonic imaging, inverse problem, image processing, and machine learning.